

# Study on the Long-term Storage Mechanism and Migration of Carbon Dioxide in the Pearl River Mouth Basin, Eastern South China Sea

Li Fangfang<sup>1\*</sup>, Cai Zhenghua<sup>1</sup>, Gao Zhenglong<sup>1</sup>, Liu Cheng<sup>1</sup>, Xuan Tao<sup>1</sup>, Ma Zhanqi<sup>1</sup>,

1 CNOOC Energy Technology & Services Limited, Tianjin, 300452, China

(\*Corresponding Author: chanel\_lf@126.com)

## ABSTRACT

This study investigates the long-term phase change, migration, and sequestration mechanisms of CO<sub>2</sub> in deep saline aquifers, using X Oilfield in the South China Sea as a case study. Through integrated laboratory experiments and numerical simulations, we demonstrate that (1) hydrodynamic and residual trapping are primarily governed by two-phase relative permeability and capillary pressure, (2) dissolution trapping is strongly influenced by temperature, pressure, and salinity conditions, and (3) mineral trapping correlates with feldspar and clay mineral content. Laboratory experiments provided essential thermodynamic and kinetic parameters for site-specific numerical simulations. The simulation results reveal that during the early injection phase, 60% of the injected CO<sub>2</sub> remains in a supercritical state while 38% dissolves into formation brine, predominantly accumulating near the wellbore and causing localized pH reduction. Over time, dissolution increases significantly, followed by mineralization reactions. After 1,000 years, mineral trapping accounts for over 21% of the total sequestered CO<sub>2</sub>.

**Keywords:** sequestration mechanism, migration and evolution law, capture and sequestration, dissolution trapping, mineral trapping

## 1. INTRODUCTION

In 2022, the United Nations Framework Convention on Climate Change stating that CCUS (Carbon Capture, Utilization, and Storage) is a critical technological means and a foundational technical guarantee for achieving the temperature control targets of the Paris Agreement under the condition that it is impossible to completely abandon fossil energy. According to statistics from the Global CCS Institute, there were 196 commercial CCUS facilities globally in 2022, with a total CO<sub>2</sub> capture

capacity exceeding 240 million tons per year. By the end of 2022, China had nearly 100 operational or planned CCUS demonstration projects, with more than half of these projects already operational. These projects have a CO<sub>2</sub> capture capacity of approximately 4 million tons per year and an injection capacity of about 2 million tons per year, representing increases of about 33% and 65% respectively compared to 2021.

As a key application scenario CCUS technology, offshore geological CO<sub>2</sub> sequestration not only serves as a viable strategy for achieving carbon emission reduction in coastal regions but also represents the most effective and promising sequestration pathway. Offshore basins boast advantages including wide distribution, large storage capacity, and high levels of safety and stability. Among China's offshore basins, the Pearl River Mouth Basin of the South China Sea demonstrates favorable characteristics for CO<sub>2</sub> sequestration, attributed to its excellent reservoir-caprock properties, substantial aquifer thickness, and significant storage potential. Furthermore, within China's coastal urban agglomerations, the Pearl River Delta region features a highly developed economy and large-scale CO<sub>2</sub> emission sources.

CO<sub>2</sub> is effectively sequestered in deep saline aquifers through complex physico-chemical reactions. This process primarily involves four distinct sequestration mechanisms: hydrodynamic trapping, dissolution trapping, mineral trapping, and residual trapping, each exhibiting unique characteristics across different time scales. However, variations in temperature, pressure conditions, mineral composition and saline water chemistry among storage sites lead to successful identification of potential deep aquifer sequestration sites requires a comprehensive understanding of all physical and chemical trapping mechanisms, as well as a thorough investigation of geological characteristics, storage economics, and

storage safety-critical factors that ensure the long-term, economic, and safe sequestration of CO<sub>2</sub>.

Numerical simulation has been widely employed by researchers to investigate long-term CO<sub>2</sub> sequestration mechanisms. Yang et al. demonstrated that hydrodynamic trapping dominates the initial stage of CO<sub>2</sub> sequestration, while mineral trapping becomes the predominant mechanism in the late stage (after 500 years of injection). Other studies by Kumar et al., Onoja et al., and Hodneland et al. have focused on parameters influencing CO<sub>2</sub> trapping and migration. Kumar specifically examined the impact of brine salinity on CO<sub>2</sub> storage, revealing that salinity significantly affects dissolution trapping but has minimal influence on mineral trapping. Onoja et al. investigated the effects of capillary pressure and relative permeability on CO<sub>2</sub> migration plumes, finding that these factors exert substantial control over hydrodynamic and residual trapping mechanisms. Notably, numerical simulation studies rely heavily on laboratory experiments to provide critical parameters and detailed physico-chemical reaction mechanisms as foundational input data.

In this study, taking the X Oilfield in the South China Sea as a case study, laboratory experiments and numerical simulations were employed to investigate the long-term phase change, migration mechanisms, and sequestration behaviors of CO<sub>2</sub>. Specifically, the contributions and reaction timescales of different sequestration mechanisms were examined. This work will provide a theoretical basis and engineering guidance for CO<sub>2</sub> sequestration project in the Pearl River Mouth Basin.

## 2. CO<sub>2</sub> TRAPPING MECHANISM IN SALINE AQUIFER

### 2.1 Basic information

The saline aquifer of the X Oilfield Group is hosted in the Hanjiang and Zhujiang Formations, with depths ranging from approximately 1,400 to 1,700m, permeability exceeding 1,000 mD, and a cumulative thickness of nearly 300 m. The aquifer has a geothermal gradient of approximately 3.54 °C/100 m, a pressure of 14.40 MPa, a formation temperature of 70.97 °C, and a salinity of 29,384 mg/L. The mineral composition and salinity characteristics of the aquifer are presented in Tables 1 and 2, respectively.

Tab.1. Saline water type and mineral composition

Cation content (mg/L)				Anion content (mg/L)				Total mineralization (mg/L)	Water type
Na <sup>+</sup>	K <sup>+</sup>	Ca <sup>2+</sup>	Mg <sup>2+</sup>	Cl <sup>-</sup>	SO <sub>4</sub> <sup>2-</sup>	CO <sub>3</sub> <sup>2-</sup>	HCO <sub>3</sub> <sup>-</sup>		
9850	292	1090	480	17266	50	0	353	29384	CaCl <sub>2</sub>

Tab.2. Mineral composition of reservoir rock

Mineral name	Quartz	Calcite	K-feldspar	Albite	Anorthite	Kaolinite	Dolomite	Smectite	Illite	Chlorite
Volume fraction,%	78	2	5	1.5	1.5	3.3	1	2.1	3.7	1.9
Specific surface area, cm <sup>2</sup> /g	9.8	-	9.8	9.8	9.8	151.6	9.8	151.6	151.6	151.6

The mechanism of CO<sub>2</sub> multi-phase evolution and sequestration in saline aquifers is not only related to the phase change of CO<sub>2</sub> under different temperature and pressure conditions, but also to the two-phase seepage law, solubility and physico-chemical reaction of CO<sub>2</sub> in saline aquifers. In order to understand the trapping mechanism and CO<sub>2</sub> migration in saline aquifers, the target oilfield core and the mineralized composition of saline water in saline aquifers were selected, and the relative permeability curve of CO<sub>2</sub>-saline water under reservoir conditions, the solubility of CO<sub>2</sub> in saline aquifer under different temperature and

pressure conditions, and the mineralization reaction were determined in the laboratory.

### 2.2 Hydrodynamic trapping and residual trapping mechanism

Using Long Core Displacement Apparatus with natural cores and formulated formation water, the two phase relative permeability curves of displacement and imbibition process. The core length is 15cm with average permeability of 600×10<sup>-3</sup>um<sup>2</sup> and average porosity of 0.25. The long core displacement tests are conducted to investigate hydrodynamic trapping and

residual trapping mechanism of CO<sub>2</sub> sequestration in aquifer.

Fig. 2 shows the relative permeability curves during CO<sub>2</sub> displacement of saline water (drainage) and saline water displacement of CO<sub>2</sub> (imbibition). As observed in the figure, CO<sub>2</sub> acts as the non-wetting phase during drainage, primarily occupying large pores, while saline water, as the wetting phase, adheres to rock surfaces and fills small pores. At the cross-point of the CO<sub>2</sub>-water relative permeability curves during drainage, the CO<sub>2</sub> saturation, water displacement efficiency, and residual

water saturation are 25.3%, 50.54%, and 49.46%, respectively. During imbibition process, saline water remains the wetting phase. Due to capillary force hysteresis, CO<sub>2</sub> trapped in pore corners, dead-end pores, or throats is immobilized by invading saline water, leading to permanent sequestration in the reservoir. At the cross-point of the CO<sub>2</sub>-water relative permeability curves during imbibition, the initial gas saturation, gas displacement efficiency, and residual saturation are 31.80%, 54.88% and 22.56%, respectively.

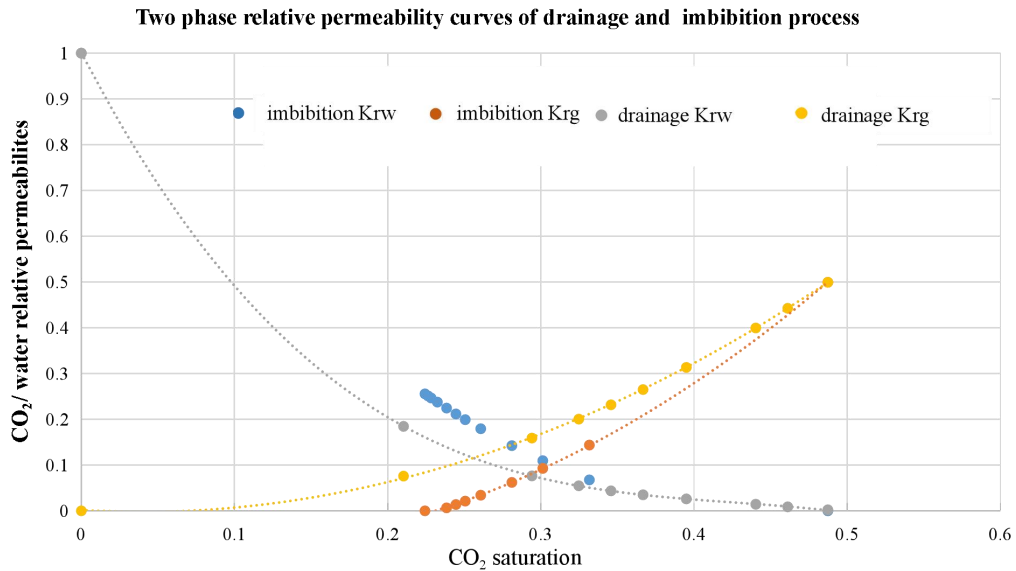


Fig. 1. Two phase permeability curve in the process of gas drive and water drive

### 2.3 Dissolution trapping mechanism

Using metering pump, high temperature and high pressure sampling device and gas flow meter, the solubility of CO<sub>2</sub> in saltwater under different temperatures and pressures was conducted, Fig.2 illustrates the testing results. As shown in the diagram, CO<sub>2</sub> solubility decreases with increasing temperature: lower temperatures correspond to higher solubility, and the decreasing trend becomes gradual once the temperature reaches a specific threshold. This phenomenon arises because elevated temperatures

increase the vapor partial pressure of CO<sub>2</sub> in saltwater, thereby reducing its solubility. At constant temperature, CO<sub>2</sub> solubility increases with pressure, as higher pressure elevates the partial pressure of CO<sub>2</sub> in the gaseous phase, promoting greater dissolution. Under identical temperature and pressure conditions, CO<sub>2</sub> solubility decreases with increasing salinity. This is attributed to the higher density caused by increased salinity, which reduces the available space for CO<sub>2</sub> dissolution.

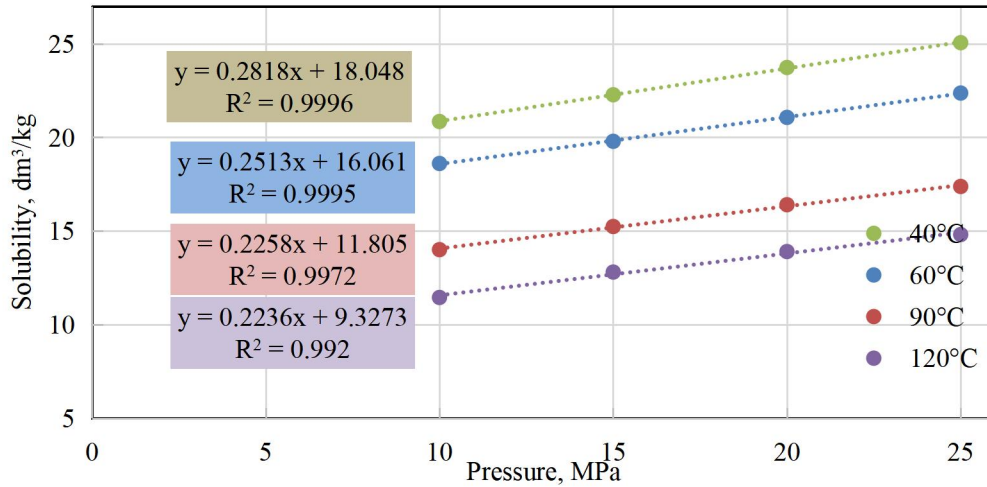


Fig. 2. CO<sub>2</sub> solubility in saline water under different temperature and pressure

#### 2.4 mineral trapping mechanism

The core rolling aging experiment was conducted in a high-temperature and high-pressure reactor device, while X-ray diffraction (XRD) measurements were performed to analyze rock minerals before and after the 30-day chemical reaction among CO<sub>2</sub>, formation water, and natural core, aiming to investigate the mineral trapping mechanism. Table 3 presents changes in rock mineral composition following the CO<sub>2</sub>-saltwater-rock reaction. As indicated in the table, the

quartz content in the rock increased after the mineralization reaction, whereas the contents of potassium feldspar, plagioclase, calcite, dolomite, and clay minerals decreased. Under reservoir temperature and pressure conditions, CO<sub>2</sub> exists in a supercritical state and primarily dissolves chlorite, calcite, dolomite, and kaolinite in the rock, while pyrite and quartz hardly react with CO<sub>2</sub>. These results demonstrate that the contents of calcite, dolomite, clay minerals, kaolinite, and chlorite are relatively reduced, while the content of quartz is relatively increased.

Tab.2. Change of rock mineral composition before and after CO<sub>2</sub>-salt water-rock reaction

Sample number	Component content (%)					
Sample	Quartz	Potassium feldspar	Plagioclase	Calcite	Dolomite	Clay mineral
No.	Q	K-F	Na-F	Ca	D	Clay
pre-experiment core	73.77	3.99	12.31	2.75	4.82	2.36
post-experiment core No.1	81.11	2.67	10.59	1.33	3.18	1.12
post-experiment core No.1	84.68	2.11	9.31	1.78	0.89	1.23
Sample	Relative content of clay minerals (%)			Mixed layer ratio (%)		
	Illite	Kaolinite	Chlorite	Illite/Smectite	Smectite	Illite
No.	I	K	C	I/S	S %	I %
pre-experiment core	23.03	23.41	1.88	51.68	75	25
post-experiment core No.1	31.55	16.23	0	52.22	75	25
post-experiment core No.1	35.11	14.05	0	50.84	75	25

### 3. LONG TERM SEQUESTRATION MACHANISM AND MIGRATION PROCESS

#### 3.1 CO<sub>2</sub>-brine-rock reaction kinetics

A core-scale simulation model using ToughReact was developed based on the hydrogeological parameters of the target saline aquifer, brine ion composition, rock mineral properties, and core physical parameters. The model incorporates experimentally measured CO<sub>2</sub> solubility equations and CO<sub>2</sub>-brine relative permeability curves to fit the variations in pressure, production, and mineral composition during CO<sub>2</sub> injection, thereby deriving the kinetic parameters of the mineralization reaction equations. The main chemical reactions and their corresponding kinetic parameters are presented in the below.

The main chemical reactions are presented in the below, and corresponding kinetic parameters listed in Table 3.

1. K-feldspar +4.0H<sup>+</sup>=2.0H<sub>2</sub>O+K<sup>+</sup>+Al<sup>3+</sup>+3.0SiO<sub>2</sub>(aq)
2. Albite+4.0H<sup>+</sup>=2.0H<sub>2</sub>O+Na<sup>+</sup>+Al<sup>3+</sup>+3.0SiO<sub>2</sub>(aq)
3. Anorthite+8.0H<sup>+</sup>=4.0H<sub>2</sub>O+Ca<sup>2+</sup>+2.0Al<sup>3+</sup>+2.0SiO<sub>2</sub>(aq)
4. Smectite+7.0H<sup>+</sup>=0.29Fe<sup>2+</sup>+3.75SiO<sub>2</sub>(aq)+0.16Fe<sup>3+</sup>+4.5H<sub>2</sub>O+1.25Al<sup>3+</sup>+0.15Na<sup>+</sup>+0.02Ca<sup>2+</sup>+0.2K<sup>+</sup>+0.9Mg<sup>2+</sup>
5. Illite+6.0H<sup>+</sup>=5.0H<sub>2</sub>O+0.6K<sup>+</sup>+0.25Mg<sup>2+</sup>+2.3Al<sup>3+</sup>+3.5SiO<sub>2</sub>(aq)
6. Kaolinite+6.0H<sup>+</sup>=5.0H<sub>2</sub>O+2.0Al<sup>3+</sup>+2.0SiO<sub>2</sub>(aq)
7. Chlorite+16.0H<sup>+</sup>=12.0H<sub>2</sub>O+5.0Mg<sup>2+</sup>+2.0Al<sup>3+</sup>+3.0SiO<sub>2</sub>(aq)
8. Calcite+H<sup>+</sup>=Ca<sup>2+</sup>+HCO<sub>3</sub><sup>-</sup>
9. Magnesite+H<sup>+</sup>=Mg<sup>2+</sup>+HCO<sub>3</sub><sup>-</sup>
10. Dolomite+2.0H<sup>+</sup>=Ca<sup>2+</sup>+Mg<sup>2+</sup>+2.0HCO<sub>3</sub><sup>-</sup>
11. Dawsonite+3.0H<sup>+</sup>=Na<sup>+</sup>+Al<sup>3+</sup>+HCO<sub>3</sub><sup>-</sup>+2.0H<sub>2</sub>O
12. Quartz=SiO<sub>2</sub>(aq)
13. Siderite+H<sup>+</sup>=HCO<sub>3</sub><sup>-</sup>+Fe<sup>2+</sup>
14. Ankerite+2.0H<sup>+</sup>=2.0HCO<sub>3</sub><sup>-</sup>+Fe<sup>2+</sup>+Ca<sup>2+</sup>

Tab. 3. List of kinetic rate parameters and equilibrium constants K at 25 °C for minerals

Mineral	Reactive Surface Area	Knetic parameters		Initial volume fraction	
		log K <sub>25</sub>	Ea	Reservoir	Cap rock
	m <sup>2</sup> /m <sup>2</sup>	mol/m <sup>2</sup> /s	kJ/mol	%	%
K-feldspar	2508.8	-12.53	38	14	7
Albite	2562.7	-12.56	69.8	2	5.5
Anorthite	2760.29	-9.12	17.8	2	5.5
Quartz	2959.04	-13.99	87.7	81	50
Illite	4188.7	-12.78	35	0.44	9.36
Kaolinite	3932.5	-13.18	22.2	0.39	5.46
Smectite	4179.61	-12.78	35	0.08	7.8
Chlorite	2957.64	-12.51	88	0.09	3.38
Calcite	2709.95	-5.81	23.5	0	6
Magnesite	3009.29	-9.34	23.5	0	0
Dolomite	2864.96	-7.63	52.2	0	0
Dawsonite	2371.6	-9.9	62.76	0	0
Siderite	3792.6	-8.89	62.76	0	0
Ankerite	3792.6	-8.89	62.76	0	0

#### 3.2 Model setup

According to the geological characteristics of the target saline aquifer, a two-dimensional actual model was established, and the reaction kinetic parameters obtained from the fitting experiment were incorporated into the model to investigate the long-term migration and evolution of CO<sub>2</sub> during long-term storage in the saline aquifer at the reservoir scale. The model has a length of 10 km and a height of 317.62 m, with a grid

size of 200×14. Two scenarios were considered: one involving the continuous distribution of seven aquifers, and the other featuring stable inter-layers between the seven aquifers. The sandstone has an average porosity of 15%~25% and a permeability of 50~500 mD, while the shale has a porosity of 0.01 and a permeability of 1 mD. The CO<sub>2</sub> injection rate was set at 30,000 tons/year, with a continuous injection period of 10 years and a total simulation duration of 1000 years.

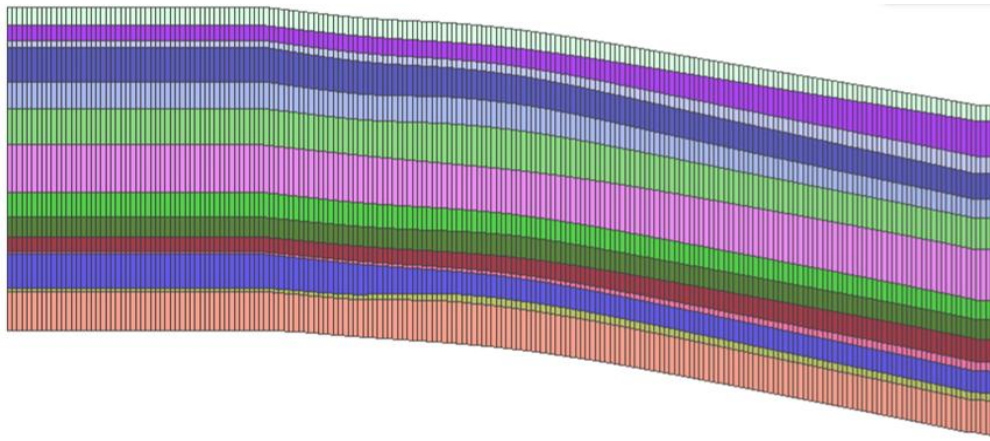


Fig. 3. 2-D actual model

### 3.3 Phase evolution and migration law

Fig.4 illustrates the phase distribution of supercritical, dissolved, and mineral CO<sub>2</sub> state within the saline aquifer after 10 and 1000 years of injection. As observed from the figure:

**Supercritical CO<sub>2</sub>:** The maximum diffusion distance reaches approximately 100 m after 10 years of injection and extends to 300 m after 1000 years.

**Dissolved CO<sub>2</sub>:** The maximum dissolution distance is about 130 m after 10 years and increases to 400 m after 1000 years.

**Mineralized CO<sub>2</sub>:** At the first 10 years of CO<sub>2</sub> injection, it predominantly existing in supercritical and

dissolved state. After 1000 years, solid CO<sub>2</sub> distributes within a 400 m range, reaching a maximum concentration of 1.6 kg/m<sup>3</sup>.

During the 1~10 year injection period, the supercritical CO<sub>2</sub> enters the reservoir and aggregated near the injection well, extensive supercritical CO<sub>2</sub> influx displaces saline water, forming a high-CO<sub>2</sub> saturation zone. In contrast, regions farther from the injection well remain unaffected by supercritical CO<sub>2</sub>, maintaining a fully saline water-saturated area. As time progresses, the supercritical CO<sub>2</sub> swept area gradually reduced, meanwhile the dissolved CO<sub>2</sub> and mineralized CO<sub>2</sub> area increased due to the dissolution and mineralization reactions.

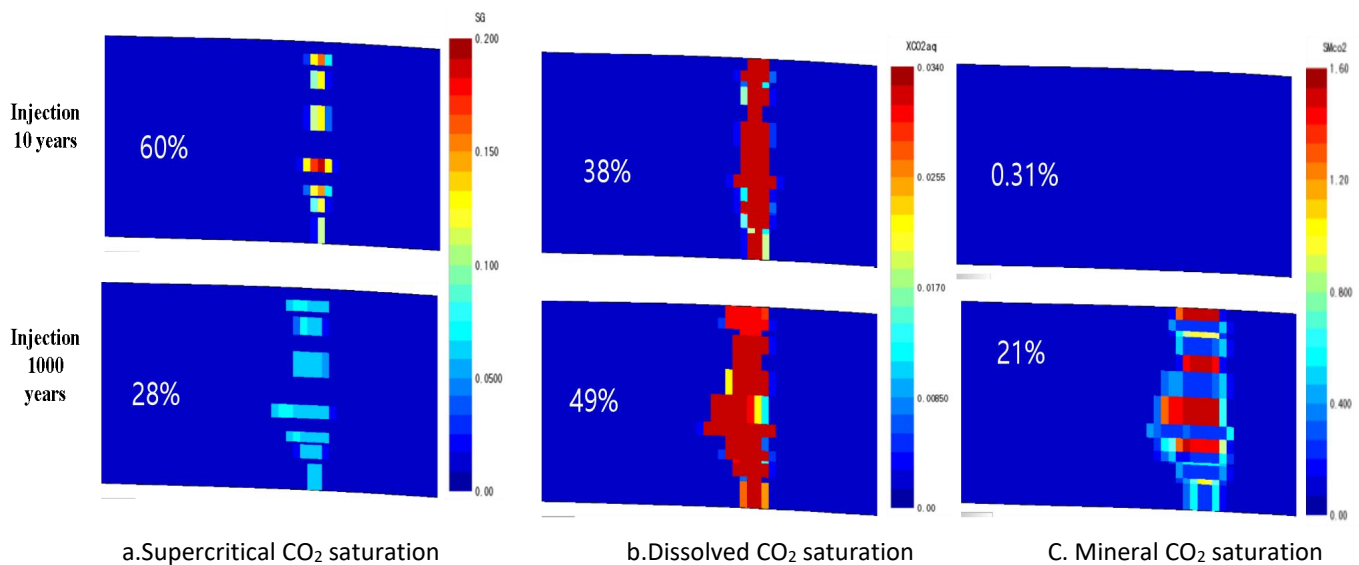


Fig. 4. Evolution of phase state during CO<sub>2</sub> injection

### 3.4 PH value change

Upon entering the reservoir, supercritical CO<sub>2</sub> dissolves in the saline water, resulting in a saline water pH decreases from 6.8 to 4.65 as shown in Fig.5. This

acidification disrupts the original water-rock reaction equilibrium, triggering a series of CO<sub>2</sub>-water-rock interactions, including the dissolution of primary minerals and precipitation of secondary minerals.

Notably, the dissolution of certain minerals consumes additional  $H^+$ , buffering the acidity of the saline water and leading to a gradual increase of pH. Over time, increased mineral participation in reactions maintains the saline water pH at a relatively elevated level. The pH

distribution area is consistent with the distribution pattern of dissolved  $CO_2$ , as pH directly reflects  $H^+$  ionization resulting from the reaction between dissolved  $CO_2$  and water.

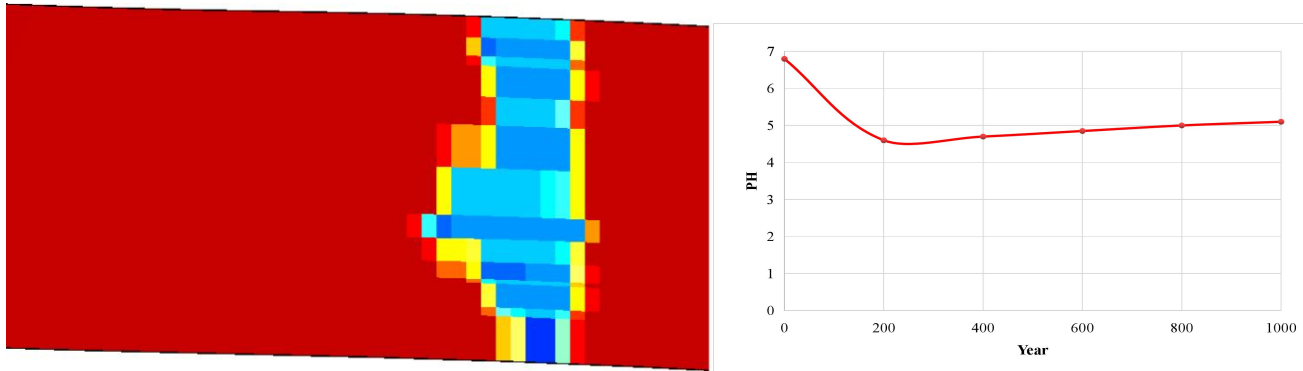


Fig. 5. PH evolution and spatial distribution diagram after 1000 years

### 3.5 Mineral changes

Fig. 5 depicts mineral evolution of albite, anorthite, kaolinite, and quartzd during the long-term storage of  $CO_2$ . The complex variations in ion concentrations during  $CO_2$  sequestration are closely linked to mineral dissolution and precipitation processes: mineral dissolution directly increases ion concentrations, with most dissolution reactions being regulated by the system's  $H^+$  availability. The onset of dissolution for each mineral is governed by its intrinsic kinetic reaction rate. The divergent reduction magnitudes of anorthite

and albite contents arise from their differing reactivity under acidic conditions. Mineral precipitation resulting from anorthite and albite dissolution primarily yields carbonate minerals, silicate minerals, and quartz, with carbonates playing a dominant role in mineral trapping. It is obvious that the initial primary minerals, namely anorthite, chlorite and smectite dissolved and Calcite, dawsonite and dolomite were the main secondary minerals during the long-term storage of  $CO_2$ .

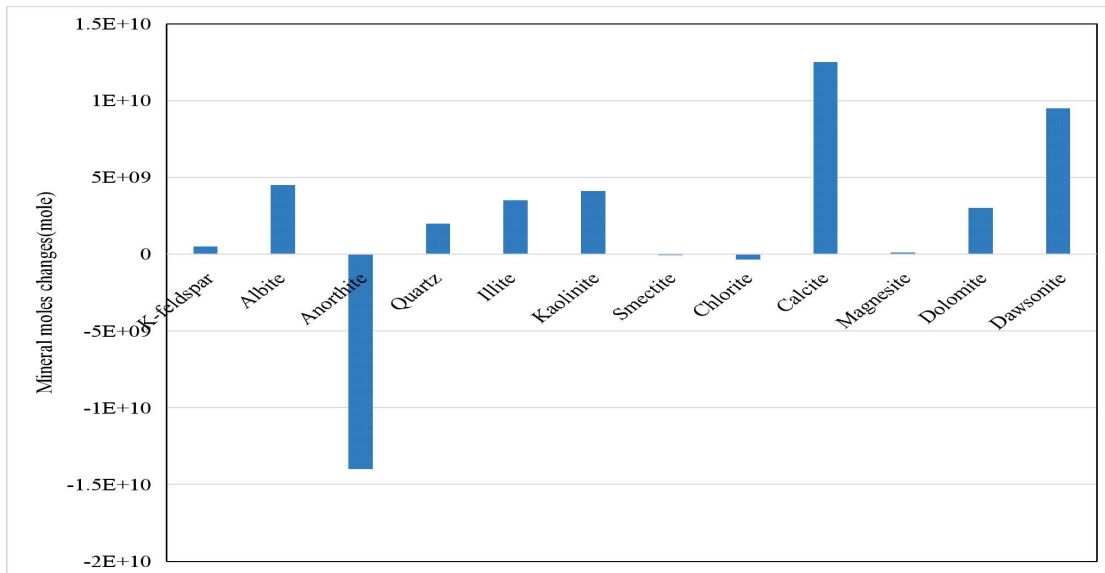


Fig. 4. Mineral changes after 1000 year

### 3.6 Sequestration volume evolution of four trapping

Table 3 presents the  $CO_2$  storage capacities evolution of four trapping mechanisms at 10 and 1000

years respectively. The total of 300,000 tons of CO<sub>2</sub> over a 10-year injection period. After 10 years, the hydrodynamic trapping contributes 37%, the residual trapping contributes 23%, the dissolution trapping contributes 38%, and Mineral trapping contributes

0.31%. At 1000 years, the hydrodynamic trapping contributes 0%, the residual trapping contributes 28%, the dissolution trapping contributes 49%, and Mineral trapping contributes 28%.

**Tab.3. Evolution of the storage capacity of four CO<sub>2</sub> storage mechanisms**

Sequestration time	There are compartments	
	10 years	1000 years
Total amount injected (ton)	300000	300000
Hydrodynamic trapping (ton)	111044(37%)	0(0%)
residual trapping (ton)	71120(23%)	110800(28%)
Dissolution trapping (ton)	116700(38%)	191500(49%)
Mineral trapping (ton)	925(0.31%)	83200(21%)

#### 4. CONCLUSIONS

In this paper, laboratory experiments and numerical simulations was adopted to study the long-term phase change, migration and sequestration mechanisms of CO<sub>2</sub> sequestration in saline aquifer in X oil field of the Pearl River Mouth Basin. The following conclusions can be generally drawn:

1. CO<sub>2</sub> Solubility Behavior: The solubility of CO<sub>2</sub> in aquifer solutions exhibits a negative correlation with temperature and salinity but a positive correlation with pressure.

2. Hydrodynamic and Residual Trapping Mechanisms: During CO<sub>2</sub>-brine displacement and imbibition processes, approximately 22.56% of injected CO<sub>2</sub> is immobilized as residual trapping within pore spaces.

3. Mineral Trapping Mechanisms: CO<sub>2</sub>-water-rock interactions lead to anorthite, chlorite and smectite dissolved and Calcite, dawsonite and dolomite were the main secondary minerals

4. Long-Term Sequestration evaluation: After 1000 years of CO<sub>2</sub> sequestration, dissolution trapping is dominant (49%), followed by residual trapping (28%) and mineralization sequestration (21%), while Hydrodynamic trapping disappears.

#### REFERENCE

[1] Zhang Xian, Yang Xiaoliang, Lu Xi. China Carbon

Capture, Utilization and Storage (CCUS) Annual Report (2023), China Management Center for Agenda 21, Global Institute of Carbon Capture and Storage, Tsinghua University, 2023.

[2] Sebastian Fischer, Axel Liebscher. CO<sub>2</sub>-brine-rock interaction-First results of long-term exposure experiments at in situ P-T conditions of the Ketzin CO<sub>2</sub> reservoir [J]. *Chemie der Erde- Geochemistry*, 2010, 70: 155-164.

[3] Galarza C, buil B. Preliminary results from the Experimental Study of CO<sub>2</sub>-Brine-Rock Interactions at Elevated T&P: Implications for the Pilot Plant for CO<sub>2</sub> Storage in Spain [J]. *Procedia Earth and Planetary Science*, 2013(7) : 272-275.

[4] Maria García-Rios, Linda Luquot. Laboratory-Scale Interaction between CO<sub>2</sub>-Rich Brine and Reservoir Rocks ( Limestone and Sandstone) [J]. *Procedia Earth and Planetary Science*, 2013( 7) : 109-112.

[5] Irina Gaus. Role and impact of CO<sub>2</sub>-rock interactions during CO<sub>2</sub> storage in sedimentary rocks [J]. *International Journal of Greenhouse Gas Control*, 2010 4( 1) : 73-89.

[6] Addisalem B Mitiku, Li D. Geochemical modelling of CO<sub>2</sub>-water-rock interactions in a potential storage formation of the North German sedimentary basin [J]. *Applied Geochemistry*, 2013, 36: 168-186.

[7] Saeko Mito, Xue Ziqiu. Geochemical Trapping of CO<sub>2</sub> in Saline Aquifer Storage: Results of Repeated Formation Fluid Sampling at the Nagaoka Site [J]. *Energy Procedia*, 2013, 37: 5449-5455.

[8] Pang Zhonghe, Li Yiman. *Geochemistry of a*

continental saline aquifer for CO<sub>2</sub> sequestration: The Guantao formation in the Bohai Bay Basin, North China [J]. Applied Geochemistry, 2012, 27( 9) :1821-1828.

[9] Pham VTH, Lu P. On the potential of CO<sub>2</sub>-water-rock interactions for CO<sub>2</sub> storage using a modified kinetic model [J]. International Journal of Greenhouse Gas Control, 2011, 5(4) : 1002-1015.

[10] Ronny Pini, Samuel C. M. Kervor, et al. Capillary pressure and heterogeneity for the CO<sub>2</sub>/water system in sandstone rocks at reservoir conditions[J]. Advances in Water Resources, 2012, 38: 48-59.

[11] Li Haiyan, Peng Shimi. Research progress on CO<sub>2</sub> sequestration mechanism in deep saline aquifer [J]. Science and Technology Review, 2013, 31 (2).

[12] Ren Shaoran, Zhang Li, Zhang Liang. CO<sub>2</sub> geological sequestration: foreign demonstration projects and their implications for China [J]. Journal of China University of Petroleum, 2010, 34 (1): 93-98.

[13] Yu Lisong, Zhang Weidong. Research progress on the dissolution and sequestration of carbon dioxide in deep saline aquifers [J]. New Energy Progress, 2015, 3 (1): 75-80.

[14] Jiang Huaiyou, Shen Pingping. Current status and prospect of carbon dioxide sequestration technology in

the world. Energy and Environment, 2010, 32 (6): 28-32.

[15] Ye Bin, Ye Weimin. Research status and prospect of CO<sub>2</sub> sequestration in saline aquifers [J]. Science and Technology Information, 2012, 36: 66-71.

[16] Peng Jialong, Chen Guanghao, Zhou Di, et al. Numerical simulation of carbon dioxide geological sequestration in Huizhou 21-1structure, Pearl River Mouth Basin [J]. Marine Geology Frontiers, 2013, 29 (9): 12.

[17] Zhao Ruirui, Meng Qinghui, Cheng Jianmei. Fluid migration simulation of CO<sub>2</sub> injection in deep saline aquifers: a case study of Sanzhao Sag, Songliao Basin [J]. Rock and Soil Mechanics, 2012, 33 (4): 7.

[18] Yu Hongwei, Li Shi, Chen Xinglong. Numerical simulation of main controlling factors of carbon dioxide sequestration in saline aquifers [J]. Science Technology and Engineering, 2012, 20 (28): 4.

[19] Wang Tao. CO<sub>2</sub> sequestration potential in saline aquifers and analysis of influencing factors [J]. Lithologic hydrocarbon reservoir, 2010, 22 (Suppl.): 85-88.

[20] HUO Chuanlin, LI Guanbao, PAN Jianming, et al. Analysis of advantages and disadvantages of CO<sub>2</sub> submarine storage in China and countermeasures and suggestions [J]. Marine Environmental Science, 2014, 33 (1): 6.